

RSC Advances



This is an *Accepted Manuscript*, which has been through the Royal Society of Chemistry peer review process and has been accepted for publication.

Accepted Manuscripts are published online shortly after acceptance, before technical editing, formatting and proof reading. Using this free service, authors can make their results available to the community, in citable form, before we publish the edited article. This *Accepted Manuscript* will be replaced by the edited, formatted and paginated article as soon as this is available.

You can find more information about *Accepted Manuscripts* in the [Information for Authors](#).

Please note that technical editing may introduce minor changes to the text and/or graphics, which may alter content. The journal's standard [Terms & Conditions](#) and the [Ethical guidelines](#) still apply. In no event shall the Royal Society of Chemistry be held responsible for any errors or omissions in this *Accepted Manuscript* or any consequences arising from the use of any information it contains.

Preparation of antiferromagnetic Co₃O₄ nanoparticles from two different precursors by pyrolytic method: *In vitro* antimicrobial activity

Totan Ghosh,^a Sandeep Kumar Dash,^b Prateeti Chakraborty,^a Averi Guha,^a Kenji Kawaguchi,^c Somenath Roy^b, Tanmay Chattopadhyay,^d * Debasis Das^{a,*}

^aDepartment of Chemistry and Centre for Research in Nanoscience and Nanotechnology, University of Calcutta, 92, A. P. C. Road, Kolkata - 700009, West Bengal, India

^bDepartment of Human Physiology with Community Health, Vidyasagar University, Midnapore-721102, West Bengal, India

^cNanosystem Research Institute, National Institute of Advanced Industrial Science and Technology (AIST), 1-1-1 Higashi, Tsukuba, 305-8565 Ibaraki, Japan

^dDepartment of Chemistry, Panchakot Mahavidyalaya, Sarbari, Neturia, Purulia- 723121, West Bengal, India

Two varieties of Co_3O_4 nano particles (Co_3O_4 -I and Co_3O_4 -II) have been synthesized from two different precursors using pyrolytic technique. Co_3O_4 -I was prepared by using a coordination polymer $[\text{Co}(\text{dca})_2(2\text{-benzoylpyridine})]_n$ (dca = dicyanamide) as sole precursor, whereas Co_3O_4 -II was obtained from a dinuclear complex $[\text{Co}_2(\text{HL})(\text{OAc})_2](\text{OAc})_2 \cdot 4\text{H}_2\text{O}$ [HL = 2,6-bis(N-ethylpiperazine-iminomethyl)-4-methyl phenol]. The synthesized nanoparticles were characterized by FTIR spectroscopy, magnetic measurements and X-ray diffraction studies. Both Co_3O_4 -I and Co_3O_4 -II are high-quality mono-dispersed, stable and defect-free nanoparticles. The surface morphology of these nanoparticles was revealed by scanning electron microscopy. Co_3O_4 -I nanoparticles have square shape and size ranging from 10 to 25 nm, whereas Co_3O_4 -II nanoparticles have hexagonal shape with larger particle size (100-150 nm). The size distribution of the nanoparticles was determined by dynamic light scattering. The particle size and microstructure were studied by transmission electron microscopy (TEM) images. These nanoparticles show an effective anti-microbial activity, employing *Staphylococcus aureus* and *Escherichia coli* as model microbial species, evidenced from the Minimum Inhibitory Concentration (MIC) and Minimum Bactericidal Concentration (MBC) values.

Introduction

Nanostructured materials have attracted intense attention due to their amazing physical and chemical properties.¹⁻³ Among the various types of nanomaterials nanostructured transition-metal oxides deserve special consideration for their outstanding properties and technological applications.⁴⁻⁷ Magnetic nanomaterials like Co_3O_4 are of great interest to the researchers from different fields like magnetic fluids, magnetic resonance imaging, biotechnology, catalysis, data storage and environmental remediation.⁸⁻¹⁵ Magnetic nanomaterials having potential application as medicine is a new arena of research which demands further exploration.¹⁶⁻¹⁹ However, synthesis of transition metal-oxide nano particles with desired properties and having environmentally stability is very difficult to achieve. Moreover the available preparative methods like hydrothermal, combustion, ultrasonic-assisted and microwave-assisted hydrothermal²⁰⁻²⁴ are costly and time consuming. We have developed a simple pyrolytic technique to prepare metal oxide nano particles employing coordination polymers or coordination complexes as sole precursors.²⁵⁻²⁷ We report herein syntheses of two varieties of Co_3O_4 nanoparticles, namely Co_3O_4 -I and Co_3O_4 -II via pyrolysis of a coordination polymer $[\text{Co}(\text{dca})_2(2\text{-benzoylpyridine})]_n$ (dca = dicyanamide) and a dinuclear complex $[\text{Co}_2(\text{HL})(\text{OAc})_2](\text{OAc})_2 \cdot 4\text{H}_2\text{O}$ [HL = 2,6-bis(N-ethylpiperazine-iminomethyl)-4-methyl phenol] respectively as sole precursor, their characterization by UV-Vis, IR, X-ray powder diffraction and variable temperature magnetic study. Morphology, size distribution and particle size have been evaluated by SEM, DLS and TEM measurements. We have further explored the antimicrobial activity of the well characterized nano scaled Co_3O_4 particles against *Staphylococcus aureus* and *Escherichia coli* as model microbial species, a study has not yet been explored well.²⁸⁻³² The objective of this study

is to develop the bactericidal effect of cobalt oxide nanoparticles using various strains. Such a study would reveal better utilization of nanoparticles for specific application.

Results and Discussion

Thermogravimetric analysis

The thermal behaviour of the precursors were examined by thermogravimetric analyses [Figure 1(a) and (b)] which reveal that Co_3O_4 species were the thermally stable end product of the pyrolytic reaction of the coordination polymer $[\text{Co}(\text{dca})_2(2\text{-benzoylpyridine})]_n$ [exp. weight loss = 81.50% (calcd. 78.55%)] and the dinuclear complex $[\text{Co}_2(\text{HL})(\text{OAc})_2](\text{OAc})_2 \cdot 4\text{H}_2\text{O}$ [exp. weight loss = 72.49% (calcd. 70.86%)].

Infrared spectroscopy analysis of metal oxide nano particles

FT-IR spectra of the thermally stable end product of the species $\text{Co}_3\text{O}_4\text{-I}$ show strong bands at about 570 cm^{-1} and 665 cm^{-1} and $\text{Co}_3\text{O}_4\text{-II}$ show strong bands at about 567 cm^{-1} and 665 cm^{-1} (Figure 2 (a) and (b)). The small band obtained at about 3422 cm^{-1} and 3434 cm^{-1} respectively due to presence of moisture in KBr. The first band is associated with the Co^{3+} vibration in the octahedral hole and the second band is attributed to the Co^{2+} vibration in the tetrahedral hole³³ which confirms the formation of the Co_3O_4 spinals.

X-ray diffraction analysis

The X-Ray powder diffraction (XRD) patterns of both Co₃O₄-I and Co₃O₄-II nanoparticles (Figure 3(a) and (b)) were produced well defined diffraction patterns, indicating that they are crystalline and the visible peaks can be well indexed to the Co₃O₄ phase³⁴. All six diffraction peaks can be assigned undisputedly to (111), (220), (400), (311), (511) and (440) lattice planes, which are in good agreement with those of the bulk Co₃O₄. There is no evidence for parasitic phases like CoO or metallic Co.

Scanning electron microscopy analysis

The morphology and particle size of the metal oxide nanoparticles were examined by SEM (Figure 4(a) & 4(b)). Square and hexagonal like morphologies for Co₃O₄-I and Co₃O₄-II have been visualized in their respective SEM micrographs with the size ranges from 10-25 nm and 100-150 nm respectively.

Dynamic light scattering

The measurement of the hydrodynamic size of Co₃O₄-I and Co₃O₄-II by dynamic light scattering shows stable nonaggregated particles with a mean diameter of 120±20 nm and 500±50 nm respectively (Figure 5(a) & 5(b)). The PDI value of Co₃O₄-I is 0.635 and for Co₃O₄-II is 0.856. The calculated size distribution histogram confirmed the size distribution of NPs. These NPs showed good stability in water.

Transmission electron microscopy

The transmission electron microscopy of Co₃O₄-I and Co₃O₄-II NPs shows nearly spherical geometry with a mean size of 30 ± 10 and 100 ± 20 nm respectively. The result is represented in Figure 6(a) & (b). The observed size of the NPs was approximately larger than the hydrodynamic diameter obtained from the DLS experiment. Transmission electron microscopy measured the size in the dried state of the sample, whereas DLS measured the size in the hydrated state of the sample, so the size measured by DLS was a hydrodynamic diameter and was larger. However, one has to bear in mind that by in transmission electron microscopy we got the images of single particle, whereas DLS gives an average size estimation, which is biased toward the larger-size end of the population distribution.

Magnetic measurements

The temperature dependence of magnetization was studied under field-cooled (FC) and zero-field-cooled (ZFC) protocols at fields of 100 Oe. The sample was first cooled down to 10 K without field and measured from 10 to 300 K (ZC: Zero-Cool measurement) with an applied field. The measurement continued from 300 to 10 K under the field (FC: Field-Cool measurement). The typical curves are suggesting antiferromagnetism behavior. Again, the Curie-Weiss ($1/\chi - T$) plots fit well the linear line above 50 K (Figure 7 (a) and (b)). We found the Weiss temperatures -117 K and -119 K for Co₃O₄-I and Co₃O₄-II respectively, which mean antiferromagnetic interaction at the ferromagnetic state. The Neel temperatures judged from the both curves peak are around 40 K which is same as the bulk Co₃O₄³⁵. These results indicate pure Co₃O₄ formation for both samples. We again performed hysteresis measurements for both

Co₃O₄-I and Co₃O₄-II samples at 10 K and 300 K but did not obtain clear hysteresis magnetization curves (SI file (S4)). These results clearly showed the absence of magnetic impurities of metallic cobalt as well as superparamagnetism behavior³⁶.

Microbial activity

MIC value determination

Co₃O₄ nanoparticles were charged against *Staphylococcus aureus* and *Escherichia coli* strains give the MIC value of 128 µg/ml and 64 µg/ml respectively (Figure 8(a) and (b)) for Co₃O₄-I and 64 µg/ml and 32 µg/ml respectively for Co₃O₄-II (SI file (S1&S2)). It may be due to the penetration of Co₃O₄ nanoparticles into the bacterial cell which may be followed by the bacteriostatic activity.

MBC value determination

Particular drug concentration was noted for each strain where no visible growth appears on agar plate of Co₃O₄ nanoparticles treatment. Co₃O₄ nanoparticles charged against *Staphylococcus aureus* and *Escherichia coli* strains give the MBC value of 128 µg/ml and 128 µg/ml, respectively [Figure 9(a) and (b)] for Co₃O₄-I and 128 µg/ml and 256 µg/ml, respectively for Co₃O₄-II (SI file (S3)). It may be due to the penetration of Co₃O₄ nanoparticles into the bacterial cell which inhibit the bacterial growth and acts as a bactericidal. Co₃O₄ nanoparticles also significantly decrease ($p < 0.05$) the cell viability of *Staphylococcus aureus* and *Escherichia coli* (Figure 10). It may be due to the transport of Co₃O₄ nanoparticles through endocytosis across the plasma membrane into the cytoplasm and kills the bacterial cell^{37, 38}.

Evidence in support of endocytosis across the plasma membrane into the cytoplasm

a. By atomic absorption spectra

We analyzed the supernatant after centrifugation of 5 mg/ml and 10mg/ml nanoparticles incubated in the bacteria culture supernatant. Figure 12 shows the Co ions released from nanoparticles. Results show that the bare Co_3O_4 - II NPs release highest ion (2368.54 ppm) than Co_3O_4 - I NPs (1895.65 ppm) This result support the internalization of the metal nanoparticles into the cell. Internalization of metal nanoparticles causes the release of Co ions into the cell and these free ions were responsible for antibacterial activity of the nanoparticles.

b. By Infrared Spectroscopic study

The bacterial cells were incubated with both the nanoparticles (previous dose of MIC level) and cell pellets were collected by centrifugation at 2400 rpm. Cells were dried and were used for spectrum analysis (Figures S5 and S6 in SI file). Figure S5 shows free cell of *Escherichia coli* and *Escherichia coli* + Co_3O_4 nanoparticles and Figure S6 shows free cell of *Staphylococcus aureus* and *Staphylococcus aureus* + Co_3O_4 nanoparticles which show a broad band at about 3450cm^{-1} due to hydroxyl groups present in the cell membrane and some characteristic bands at about $1300\text{-}1600\text{ cm}^{-1}$. When Co_3O_4 nanoparticles were treated with the bacterial cell, then the above indicated bands are almost vanished due to the interaction of the nanoparticles with the

cell wall and new bands at about 570 cm^{-1} and 665 cm^{-1} are observed due to the characteristics metal-oxygen bonding vibration.

The cytocompatibility of the nanoparticles with eukariote/ human cells

The cytotoxic activity of Co_3O_4 nanoparticles on human lymphocytes was evaluated by assessing the cell viability using a standard MTT assay method (Figure 11). Cells were treated with different concentration of Co_3O_4 nanoparticles ($50\text{ }\mu\text{g/ml}$ to $800\text{ }\mu\text{g/ml}$). It was found that there was no significant difference ($P < 0.05$) in cell viability up to $200\text{ }\mu\text{g/ml}$ dose of both Co_3O_4 nanoparticles in respect with control indicated as a safe dose for bio-medical applications.

Experimental

Materials

All chemicals were obtained from commercial sources and used as received. Solvents were dried according to standard procedure and distilled prior to use³⁹. 2-benzoyl pyridine, sodium dicyanamide, *N*-(2-aminoethyl) piperazine were purchased from sigma-aldrich, Cobalt perchlorate hexahydrate and cobalt acetate dihydrate obtained from Merck Ltd. and used as received. 2,6-diformyl-4-methyl-phenol was prepared according to the literature method⁴⁰. Sodium chloride, Luria broth, nutrient agar, agar powder, Mueller-Hinton broth, cell culture grade dimethyl sulfoxide (DMSO), RPMI-1640, fetal bovine serum (FBS), penicillin, streptomycin, L-glutamine were purchased from Himedia, India. KH_2PO_4 , K_2HPO_4 , alcohol and other chemicals were procured from Merck Ltd., SRL Pvt. Ltd., Mumbai, India. All other chemicals used were of AR grade.

Physical measurements

To determine the structural features of the samples, Fourier transform infrared (FTIR) spectroscopy was carried out at 25 °C using a PERKIN-ELMER SPECTRUM RXIFT-IR SYSTEM FT-IR spectrometer with 64 scans for wave numbers ranging from 400 to 4000 cm^{-1} and resolution 4 cm^{-1} . The KBr pellet method was used to prepare the samples. Electronic spectra (200-1200nm) were obtained at 25°C using a U-3501 HITACHI, JAPAN. Thermal analyses (TGA) were carried out on a TGA/SDTA851^e METTLER - TOLEDO thermal analyzer where the samples were heated from room temperature to 600°C under flowing nitrogen atmosphere (flow rate: 40 $\text{cm}^3 \text{min}^{-1}$) at a heating rate of 10°C/min in a platinum crucible. The morphology and size of Co_3O_4 particles have been characterized by scanning electron microscopy (SEM) (Hitachi S-3400N) operating at 15 kV. All samples were coated with a thin layer of gold before examining. The size distribution of the nanoparticles were determined by dynamic light scattering (DLS; Zetasizer Nano ZS; Malvern Instruments, Malvern, UK). The particle size and microstructure were studied by transmission electron microscopy (TEM) with a JEOL (Japan) JEM 2100 high-resolution transmission electron microscope operating at 200 kV. In brief, the nanoparticles were suspended in deionized water at a concentration of 1 mg/mL, and then the sample was sonicated using a sonicator bath until the sample formed a homogeneous suspension. For size measurement, sonicated stock solution of all nanoparticles (0.5 mg/mL) was diluted 20 times. A drop of aqueous nanoparticles suspension was placed onto a carbon-coated copper grid and this was dried in air to obtain transmission electron Microscopy. The powder XRD measurements were carried out using Bruker D8 Advance X-ray Diffractometer. The X-rays were produced using a sealed tube and the wavelength of X-ray was 0.154 nm (Cu-K_α). To determine the crystallinity of the sample using operating voltage = 40 kV

and operating current =40 mA and $2\theta = 20^\circ$ - 80° . The magnetic measurements of the Co_3O_4 particles were carried out using SQUID magnetometer (Quantum Design MPMS). The measurement temperature was between 10 and 300 K with the maximum applied field +/- 1 T.

Biological measurements

Bacterial strain

Staphylococcus aureus strains were clinically isolated from postoperative pus samples of patients admitted to Burn and Wound section of Midnapore Medical College and Hospital, Midnapore, West Bengal, India during a three month period from December 15, 2008 to June 15, 2009⁴¹. *Escherichia coli* also clinically isolated from UTI patient's urine samples during a two month period from November 15, 2010 to January 15, 2011⁴². These strains were used in this study to evaluate whether or not cobalt oxide nanoparticles have antimicrobial activity. Bacterial culture was done in Mueller-Hinton broth at 37°C throughout the experiment.

Dose of cobalt oxide nanoparticles for antimicrobial study

Several doses (2 $\mu\text{g}/\text{ml}$ -128 $\mu\text{g}/\text{ml}$) of Co_3O_4 nanoparticles were prepared using sterile PBS pH 7.4. In this study, all these doses were charged against *Staphylococcus aureus* and *Escherichia coli*.

Determination of Minimum Inhibitory Concentration

The MIC values of Co_3O_4 nanoparticles were determined by a broth dilution method using Mueller-Hinton broth (MHB), as recommended by the National Committee for Clinical Laboratory Standards (NCCLS), 2000⁴³. About 5×10^4 cells in MHB were treated with different

concentrations of nanoparticles and shaken for 16 h at 37°C. The minimum concentration at which there was no visible turbidity was taken as the MIC value.

Determination of Minimum Bactericidal Concentration

The MBC values of Co₃O₄ nanoparticles were determined according to Okore, 2005⁴⁴. This is an extension of the MIC Procedure. Bacterial culture used for the MIC test were inoculated onto the Mueller–Hinton agar and incubated at 37°C for 24 h. Microbial growth or death was ascertained via no growth on Mueller–Hinton agar plate. The minimal concentration of the Co₃O₄ nanoparticles that produced total cell death is the MBC.

Cell Viability Assay

Cell viability of *Staphylococcus aureus* and *Escherichia coli* was performed by 3-(4, 5-dimethylthiazol-2-yl)-2,5 diphenyltetrazolium bromide (MTT) method according to Mosmann, 1983⁴⁵ after 12 h of treatment with Co₃O₄ nanoparticles. Drug treated (1 X MIC) bacterial cultures were centrifuged at 2400 rpm for 10 min followed by repeated washing for two times with phosphate buffer (pH-7.4). The volume of phosphate buffer is used for each washing step is 500µl. Thereafter, the medium was replaced with fresh RPMI (without Phenol Red and FBS) containing 0.5 mg/ml of MTT. After additional 3 hrs incubation at 37°C, HCl-isopropanolic solution was added and after 15 min of incubation at room temperature, absorbance of solubilized MTT formazan product was spectrophotometrically measured at 570 nm. Further cell viability assay of both the bacteria was performed by crystal violet assay⁴⁶. In this assay after co-culture, each cell was washed with sterile saline to remove the macrophages and dead cells. The surviving cells were stained with 0.1 % crystal violet/ methanol at room temperature for 10

min. The plates were read on a microplate reader (model 550, Bio-Rad, Tokyo, Japan) at a wavelength of 570 nm. Cytolysis was calculated as a percentage. The absorbance of surviving cells (control absorbance) was set at 100 %, and the experimental absorbance was divided by the control absorbance⁴⁷.

The cytocompatibility of the nanoparticles with human cells

Isolation of normal human lymphocytes

Fasting blood samples were collected from a healthy individual satisfying the Helsinki protocol. The lymphocytes were isolated from Heparinized blood samples according to the method of Hudson and Hay, 1991⁴⁸. Blood taken was diluted with phosphate-buffered saline (pH 7.0) in equal ratio and then layered very carefully on the density gradient (histopaque) in 1:2 ratio, centrifuged at 500X g for 20 min and the white milky layer of mononuclear cells, i.e., lymphocytes were carefully removed. The layer was washed twice with the same buffer and then centrifuged at 3,000X g for 10 min to get the required pellet of lymphocytes and cultured in RPMI-1640 medium supplemented with 10% FBS, 100 units/ml penicillin, 100µg/ml streptomycin and 4 mM L-glutamine under 5% CO₂ and 95% humidified atmosphere at 37 °C.

In Vitro Cytotoxicity assay of Co₃O₄ nanoparticles

Cellular cytotoxicity assay was performed by 3-(4, 5-dimethylthiazol-2-yl)-2,5 diphenyl tetrazolium bromide (MTT) method according to Mosmann⁴⁵. The human lymphocytes were cultured in RPMI 1640 medium supplemented with 10% FBS, 100 units/ml penicillin, 100µg/ml

streptomycin and 4 mM L-glutamine under 5% CO₂ and 95% humidified atmosphere at 37 °C. Cells were seeded into 96 wells of tissue culture plates having 180 µl of complete media and were incubated for 18 h. Co₃O₄ nanoparticle was added to the cells at different concentrations (50 µg/ml – 800 µg/ml) were incubated for 72 h at 37 °C in a humidified incubator maintained with 5% CO₂. Thereafter, the medium was replaced with fresh RPMI (without FBS) containing 0.5 mg/ml of MTT. After additional 3 h incubation at 37 °C, HCl-iso propanolic solution was added to each culture plates. After 15 min of incubation at room temperature, absorbance of solubilized MTT formazan product was measured spectrophotometrically at 570 nm.

Cobalt ion release assay by atomic absorption spectroscopy (AAS)

Co₃O₄- I and Co₃O₄- II nanoparticles were suspended in the media containing bacteria (2X10⁵ CFU/ml) and incubate for 24 hour at 37⁰C. After the incubation period, the supernatant was used for the estimation of free cobalt ions in the medium by atomic absorption spectroscopy (Simatzu AA7000) using different concentration (ppm) of CoCl₂.6H₂O as standard ⁴⁹.

Preparation of Co₃O₄ nanoparticles

Co₃O₄-I and Co₃O₄-II nanoparticales were prepared by heating polymeric complex [Co(dca)₂(2-benzoylpyridine)]_n and dinuclear complex [Co₂(HL)(OAc)₂](OAc)₂.4H₂O respectively at 480°C for two hours. Both the precursor complexes were obtained as pure single crystals adopting the procedure as reported previously ^{25, 50}. To prepare large amounts of Co₃O₄ nanoparticles from both the complexes, about 5 gm weight of each complex was heated at a constant temperature of 480 °C for two hours in big platinum crucibles separately in a muffle furnace. The obtained Co₃O₄ nanoparticles were then washed with methanol followed by water to remove the impurity.

The pure Co_3O_4 nanoparticles thus obtained were characterized by FT-IR spectroscopy, magnetic measurement, powder XRD and SEM images.

Conclusion

In summary, we have prepared antiferromagnetic Co_3O_4 nanoparticles namely Co_3O_4 -I and Co_3O_4 -II using two different precursors, a coordination polymer and a dinuclear coordination complex respectively, by a simple pyrolytic technique without using any catalyst or template. Although morphology and shape of those two varieties cobalt oxide nanoparticles are more or less identical, they are differ widely in the size as are evidenced from TEM, SEM and DSL measurements. Variable temperature magnetic study reveals that both Co_3O_4 nanoparticles are antiferromagnetic in nature. These antiferromagnetic Co_3O_4 nanoparticles have shown an effective anti-microbial activity against *Staphylococcus aureus* and *Escherichia coli* as are evidenced from MIC and MBC values. The reason behind the effectiveness of Co_3O_4 nanoparticles as antimicrobial agent is supposed to be due to the interaction of nanoparticles through endocytosis across the plasma membrane into the cytoplasm. This study shows that antiferromagnetic Co_3O_4 nanoparticles have great promise as antimicrobial agent against *E. coli* and *S. aureus* and may be used as anti-microbial agents for the treatment of gram positive and gram negative bacteria.

Acknowledgment

The instrumental support obtained from the Centre for Research on Nano Science and Nano Technology (CRNN), University of Calcutta is gratefully acknowledged. We also thankful to UGC, New Delhi [UGC Major Research Project F. No. 34-308/2008 (SR) Dated: 31.12.2008 (DD), and UGC-RFSMS project (TG)] for financial support.

References

- [1] A.T. Bell, *Science*, 2003, **299**, 1688-1691.
- [2] M. G. Fernandez, A. A. Martinez, J. C. Hanson, J. A. Rodriguez, *Chem. Rev.*, 2004, **104**, 4063-4104.
- [3] S. Sun, C. B. Murry, D. Weller, L. Folks, A. Moser, *Science*, 2000, **287**, 1989-1992.
- [4] T. Ozkaya, A. Baykal, M. S. Toprak, Y. Koseoglu, S. Z. Durmu, *J. Magn. Mater.*, 2009, **321**, 2145-2149.
- [5] B. Liu, H. C. Zeng, *J. Am. Chem. Soc.* 2004, **126**, 16744-16746.
- [6] J. J. Teo, Y. Chang, H. C. Zeng, *Langmuir*, 2006, **227**, 369-7377.
- [7] M.S. Niasari, N. Mir and F. Davar, *J. Phys. Chem. Solids*, 2009, **70**, 847-852.
- [8] W.W. Wang, Y. J. Zhu, *Mater. Res. Bull.* 2005, **40**, 1929-1935.
- [9] S.C. Petitto, E.M. Marsh, G.A. Carson and M.A. Langell, *J. Mol. Catal. A, Chem.* 2008, **281**, 49-58.

- [10] L. Sun, H. Li, L. Ren and C. Hu, *Solid State Sci.* 2009, **11**, 108-112.
- [11] P. Torelli, E. A. Soares, G. Renaud, S. Valeri, X.X. Guo, P. Luches, *Surf. Sci.* 2007, **601**, 2651-2655.
- [12] X. Xie, Y. Li, Z. Q. Liu, M. Haruta and W. Shen, *Nature*, 2009, **458**,746-749.
- [13] J. Park, X. Shen and G. Wang, *Sens. Actuators B, Chem* ,2009, **136**, 494-498.
- [14] W.Y. Li , L.N. Xu and J. Chen, *Adv. Funct. Mater.* 2005, **15**, 851-857.
- [15] B. Solsona, T. E. Davies, T. Garcia, A. Dejoz and S.H. Taylor, *Appl. Catal. B, Environ.* 2008, **84**, 176-184.
- [16] Q. A. Pankhurst, J. Connolly, S.K Jones and J. Dobson, *J. Phys. D: Appl. Phys.* 2003, **36**, R167-R181.
- [17] G. Ren, D. Hu, E. W. C. Cheng, M. A. Vargas-Reus, P. Reip and R.P.Allak, *Int. J. Antimicrobial Agents*, 2009, **33(6)**, 587-590.
- [18] N.Tran, A. Mir, D. Mallik, A. Sinha, S. Nayar and T.J. Webster, *Int. J. Nanomedicine*, 2010, **5**, 277-283.
- [19] S. Tripathi, G. K. Mehrotra and P. K. Dutta, *Bull Mater Sci*, 2011, **34(1)**, 29-35.
- [20] Y. Zhang, Y. Chen, T. Wang, J. Zhou and Y. Zhao, *Microporous Mesoporous Mater.* 2008, **114**, 257-265.
- [21] P. J. Zhan, *Alloys Compd.* 2009, **478**, 823-826.
- [22] R. K. Venkatesvara and C. S. Sunandana , *Solid State Commun.*, 2008, **148**, 32-37.

- [23] W.H. Li, *Mater. Lett.* 2008, **62**, 4149-4151.
- [24] A. Askarinejad and A. Morsali, *Ultrason. Sonochem.* 2009, **16**, 124-131.
- [25] T. Ghosh, T. Chattopadhyay, S. Das, S. Mondal, E. Suresh, E. Zangrando and D. Das, *Cryst. Growth & Des.* 2011, **11**, 3198-3205.
- [26] S. Mondal, T. Chattopadhyay, S. K. Neogi, T. Ghosh, A. Banerjee, D. Das, *Materials Letters*, 2011, **65**, 783-785.
- [27] S. Mondal, T. Chattopadhyay, S. Das, S. R. Maulik, S. Neogi and D. Das, *Indian J. Chem. Sec. A*, 2012, **51A**, 807-811.
- [28] M. Rai, A. Yadav and A. Gade, *Biotechnology Advances*, 2009, **27**, 76–83.
- [29] A. R. Shahverdi, A. Fakhimi, H. R. Shahverdi and S. Minaian, *Nanomedicine: Nanotechnology, Biology, and Medicine*, 2007, **3**, 168–171.
- [30] B.S. Inbaraj, T.Y.Tsai and B. H. Chen, *Sci. Technol. Adv. Mater.*, 2012, **13**, 015002 (8pp).
- [31] N. Tran, A. Mir, D. Mallik, A Sinha, S, Nayar and T.J. Webster, *International Journal of Nanomedicine*, 2010, **5**, 277–283.
- [32] X. L. Cao, C. Cheng, Y. L. Ma and C. S. Zhao, *J. Mater. Sci: Mater Med*, 2010, **21**, 2861–2868.
- [33] N.T. Mcdevitt and W.L. Baun, *Spectrochimca Acta*, 1964, **20**, 799-808.

- [34] I. Manoucheri, P. Kameli and H. Salamati, *J. Supercond. Nov. Magn.* 2011, **24**, 1907-1910.
- [35] W. L. Roth, *J. Phys. Chcm. Solids*, 1964, **25**, 1-10.
- [36] V. Bisht, K. P. Rajeev, *Solid State Communications* , 2011, **151**, 1275-1279.
- [37] G. J. R. Jones, *Adv. Drug. Deliv. Rev.*, 1996, **20**, 83-97.
- [38] I. Tamai and A. Tsuji, *Adv. Drug. Deliv. Rev.*, 1996, **20**, 5-32.
- [39] D. D. Perrin, W. L. F. Armario and D. R. Perrin, *Purification of Laboratory Chemicals*, Second edn, Pergamon Press, Oxford, 1980.
- [40] R. R. Gagne, C. L. Spiro, T. J. Smith, C. A. Hamann, W. R. Thies, A. K. Shiemeke, *J. Am. Chem. Soc.*, 1981, **103**, 4073-4081.
- [41] S. P. Chakraborty, S. Kar Mahapatra, M. Bal and S. Roy, *Al Ameen J. of Med. Sc.* 2011, **4(2)**, 152-168.
- [42] S. K. Dash, S. P. Chakraborty, D. Mandal and S. Roy, *International Journal of Life Science and Pharma Research*, 2012, **2(1)**, 25-39.
- [43] NCCLS. *Methods for Dilution Antimicrobial Susceptibility Tests for Bacteria that Grow Aerobically*, 5th edn, **17**, no. 2. Approved standard M7-A5. Wayne, PA: NCCLS 2000.
- [44] V. C. Okore, *Pharmaceutical microbiology* , 2005, **55**, 120.
- [45] T. Mosmann, *J. Immunol. Methods*, 1983, **65**, 55-63.

- [46] S. Chattopadhyay, S. K. Dash, T. Ghosh, S. Das, S. Tripathy, D. Mandal, D. Das, P. Pramanik and S. Roy, *J. Biol. Inorg. Chem.*, 2013, DOI 10.1007/s00775-013-1044-y.
- [47] T. Staudinger, E. Presterl, W. Graninger, G.J. Locker, S. Knapp, K. Laczika, G. Klappacher, B. Stoiser, A. Wagner, P. Tesinsky, H. Kordova and M. Frass, *Intensive Care Med.* 1996, **22**,888-893.
- [48] L. Hudson, and F. C. Hay, *Practical immunology*, 3rd, Ed. Blackwell scientific publications; Oxford/London/ Edinburgh/Boston/Melbourne: Blackwell Scientific Publications 1991, 21-22.
- [49] J. Hahn, A. Fuhlrott and S. L. Barcikowski, *J. Nanopart. Res.* 2012, **14**, 686-695.
- [50] A. Banerjee, A. Guha, J. Adhikary, A. Khan, S. Dey, E. Zangrando and D. Das, *Polyhedron*, 2013, <http://dx.doi.org/10.1016/J.Poly.2013.05.014>.

Captions for Figures

Fig.1 TGA diagram of (a) polymeric complex $[\text{Co}(\text{dca})_2(2\text{-benzoylpyridine})]_n$ and (b) dinuclear complex $[\text{Co}_2(\text{HL})(\text{OAc})_2](\text{OAc})_2 \cdot 4\text{H}_2\text{O}$.

Fig. 2 IR spectrum of (a) $\text{Co}_3\text{O}_4\text{-I}$ nanoparticle and (b) $\text{Co}_3\text{O}_4\text{-II}$ nanoparticle.

Fig. 3 XRD pattern of (a) $\text{Co}_3\text{O}_4\text{-I}$ nanoparticle and (b) $\text{Co}_3\text{O}_4\text{-II}$ nanoparticle.

Fig. 4 SEM images of (a) $\text{Co}_3\text{O}_4\text{-I}$ and (b) $\text{Co}_3\text{O}_4\text{-II}$ nanoparticles.

Fig. 5 Dynamic light scattering of (a) $\text{Co}_3\text{O}_4\text{-I}$ (b) $\text{Co}_3\text{O}_4\text{-II}$

Fig. 6 Transmission electron microscopy images of (a) $\text{Co}_3\text{O}_4\text{-I}$ (b) $\text{Co}_3\text{O}_4\text{-II}$

Fig. 7 The Curie-Weiss ($1/\chi - T$) plots fit well the linear line above 50 K.

Fig. 8 Minimum inhibitory concentration of $\text{Co}_3\text{O}_4\text{-I}$ nanoparticles against (a) *Staphylococcus aureus* and (b) *Escherichia coli* [Here A = $2\mu\text{g/ml}$, B = $4\mu\text{g/ml}$, C= $8\mu\text{g/ml}$, D= $16\mu\text{g/ml}$, E= $32\mu\text{g/ml}$, F= $64\mu\text{g/ml}$ and G= $128\mu\text{g/ml}$.]

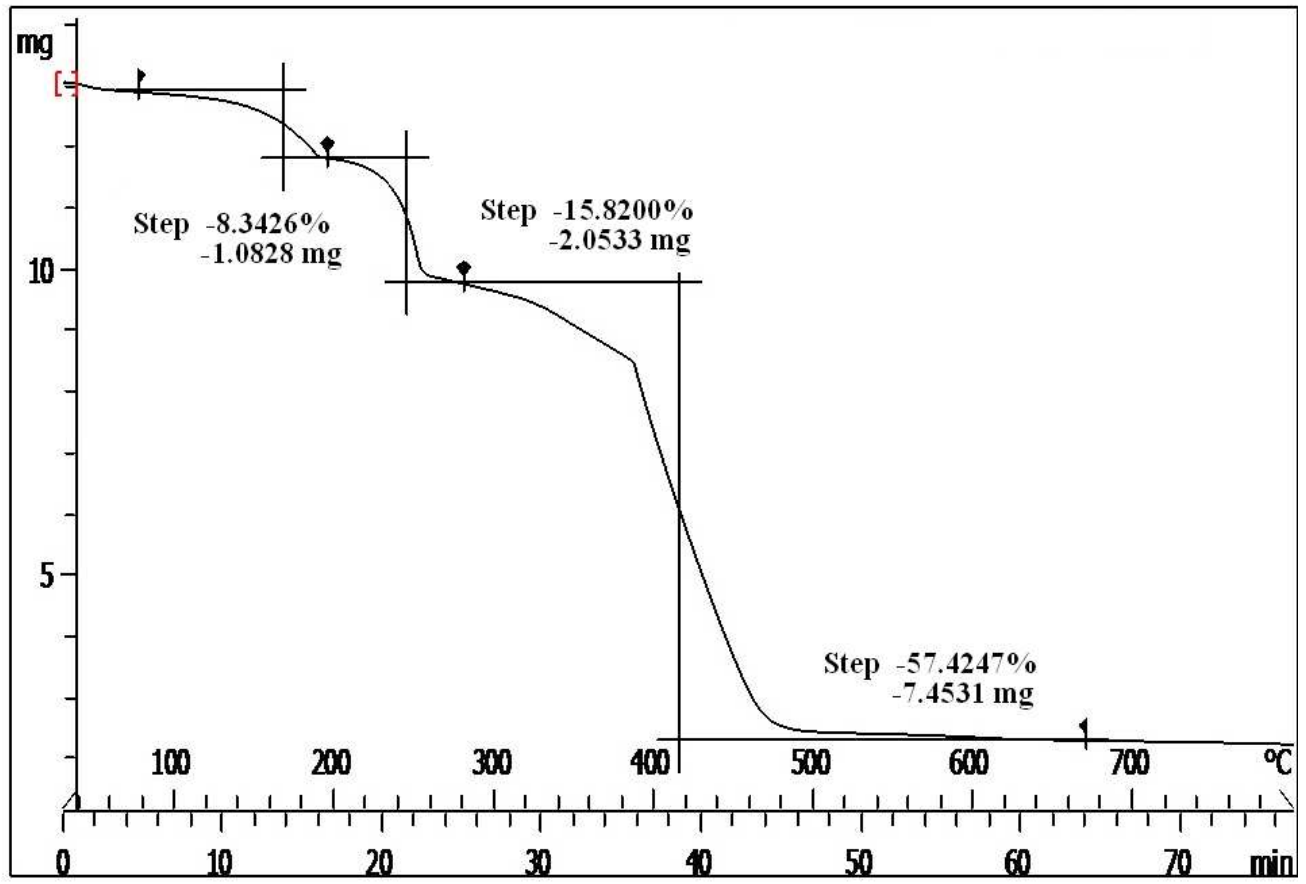
Fig.9 Minimum bactericidal concentration of $\text{Co}_3\text{O}_4\text{-I}$ nanoparticles against (a) *Staphylococcus aureus* and (b)*Escherichia coli* [Here A= $2\mu\text{g/ml}$, B= $4\mu\text{g/ml}$,C= $8\mu\text{g/ml}$, D= $16\mu\text{g/ml}$, E= $32\mu\text{g/ml}$, F= $64\mu\text{g/ml}$ and G= $128\mu\text{g/ml}$.]

Fig. 10 Cell viability of *Staphylococcus aureus* and *Escherichia coli* due to treatment of Co_3O_4 nanoparticles

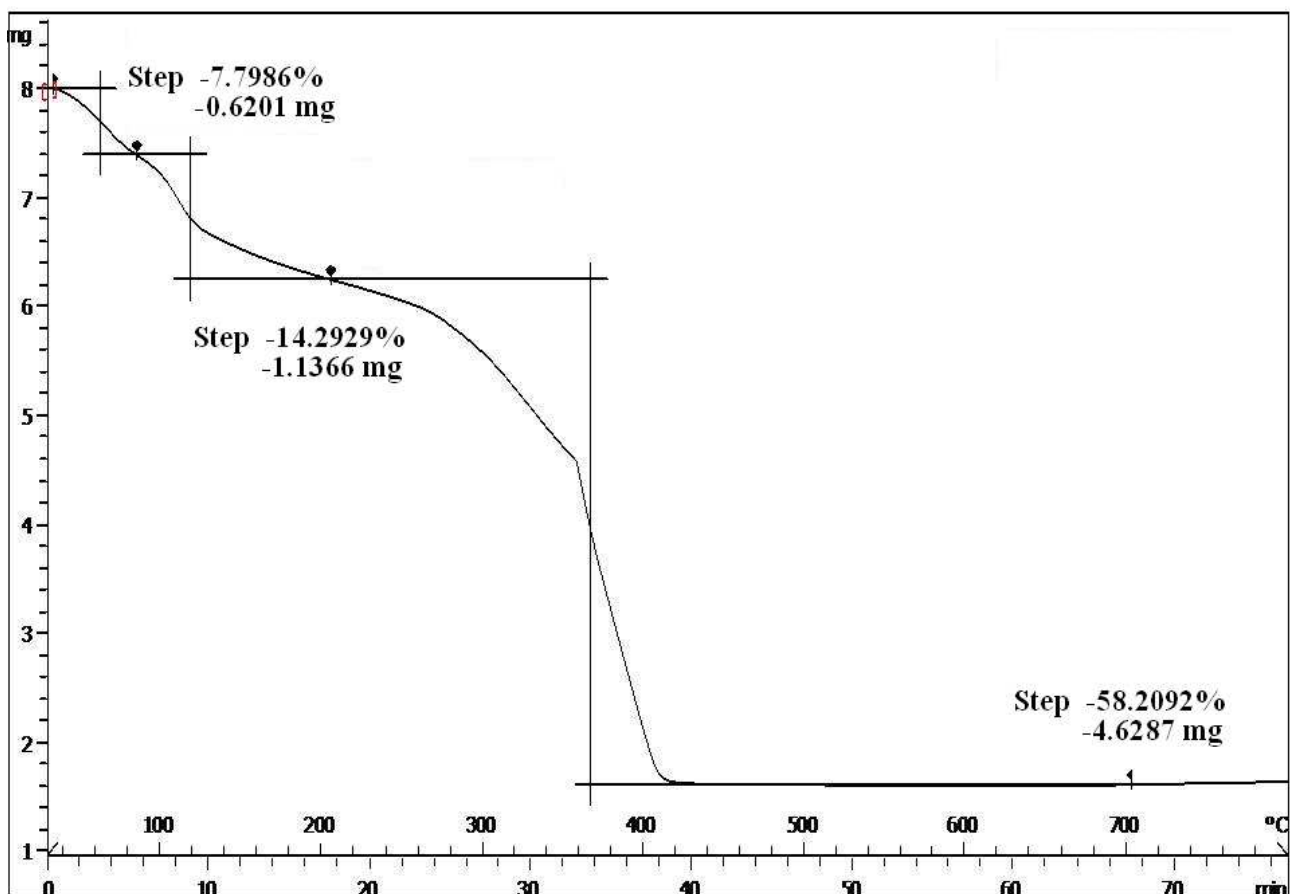
Fig. 11 Cytotoxicity of Co_3O_4 nanoparticles ($50\mu\text{g/ml}$ to $800\mu\text{g/ml}$) against human normal Lymphocytes by MTT assay.

Fig. 12 Cobalt ion release assay by atomic absorption spectroscopy (AAS).

Figure list



(a)



(b)

Fig.1 TGA diagram of (a) polymeric complex $[\text{Co}(\text{dca})_2(2\text{-benzoylpyridine})]_n$ and (b) dinuclear complex $[\text{Co}_2(\text{HL})(\text{OAc})_2](\text{OAc})_2 \cdot 4\text{H}_2\text{O}$.

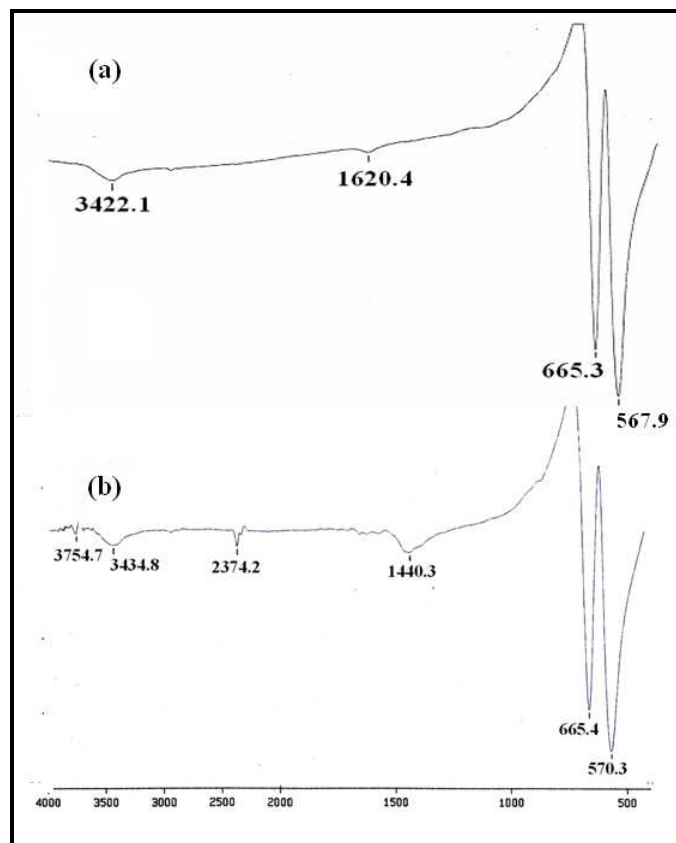


Fig. 2 IR spectrum of (a) Co₃O₄-I nanoparticle and (b) Co₃O₄-II nanoparticle.

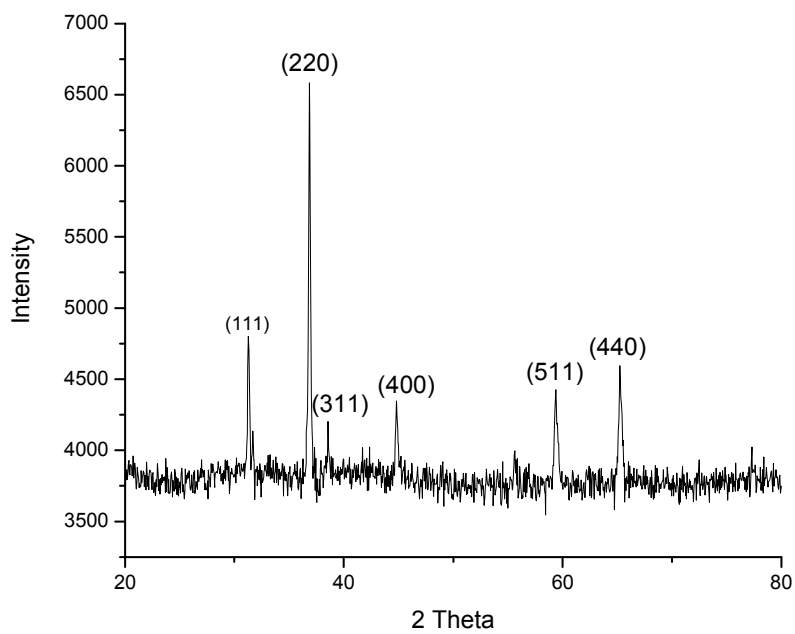
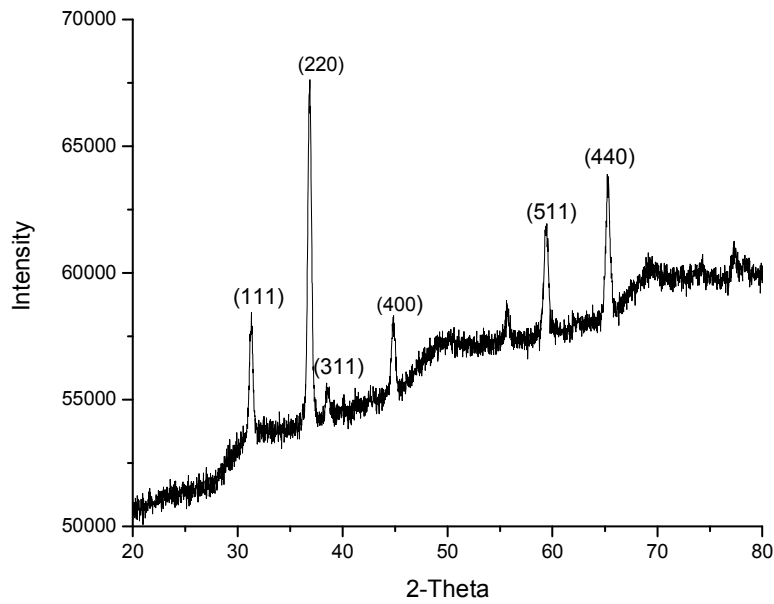
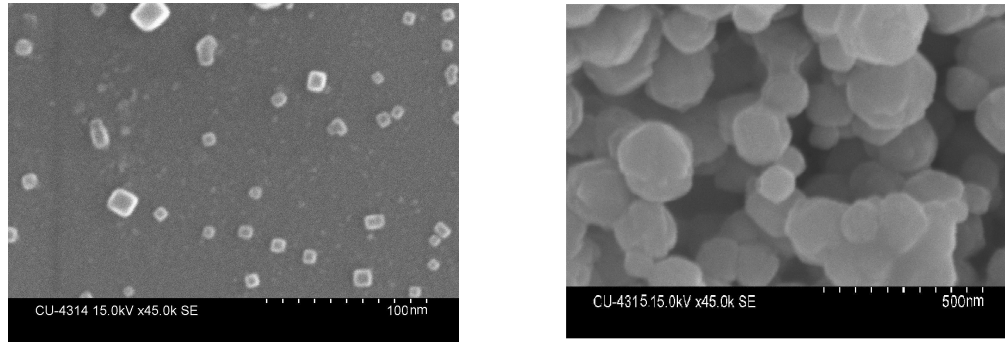
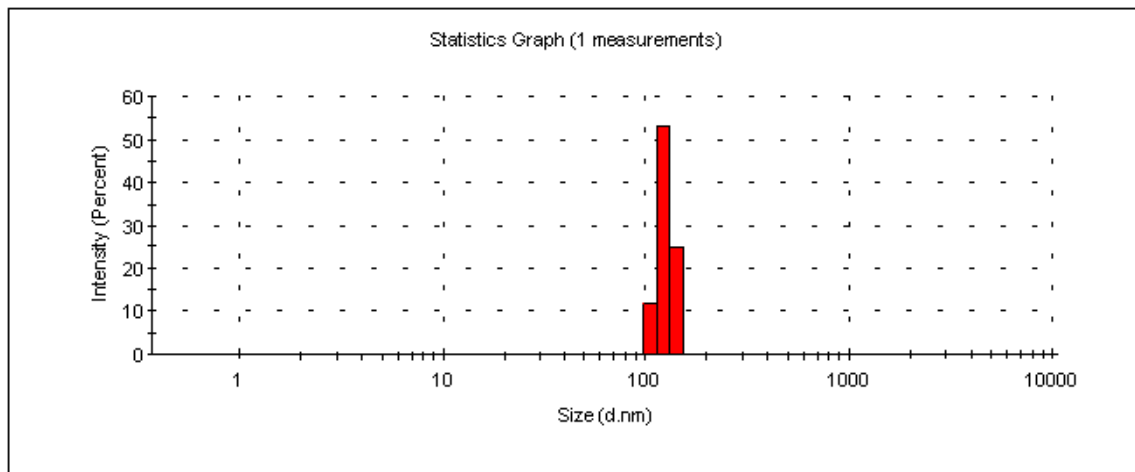
**(a)****(b)**

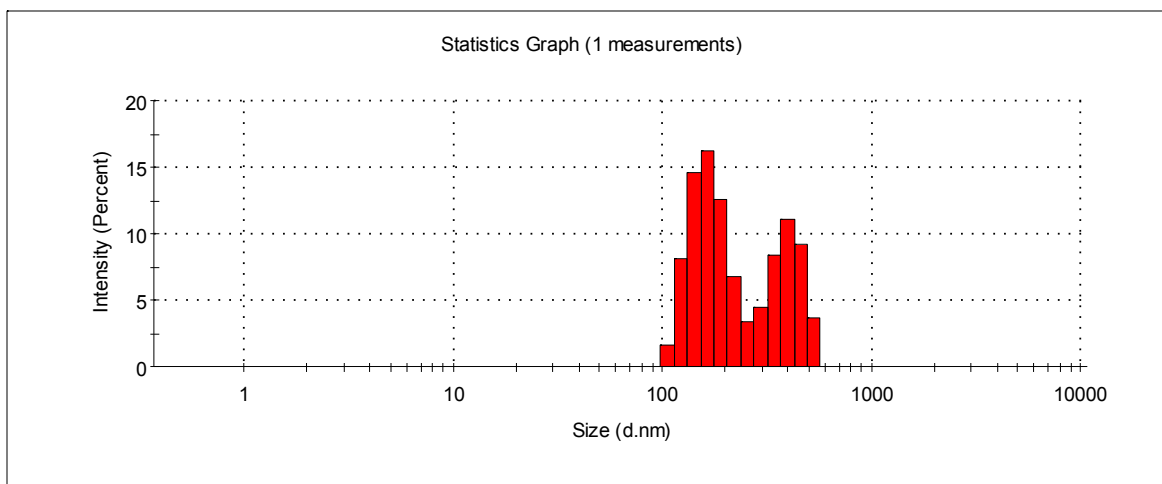
Fig. 3 XRD pattern of (a) Co₃O₄-I nanoparticle and (b) Co₃O₄-II nanoparticle.



(a) **(b)**
Fig. 4 SEM images of (a) Co₃O₄-I and (b) Co₃O₄-II nanoparticles.

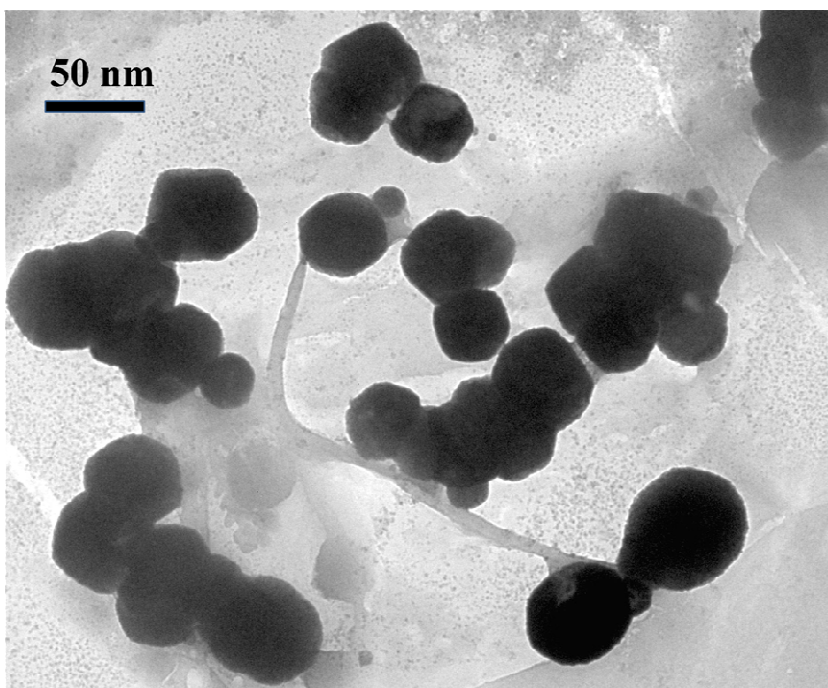


(a)

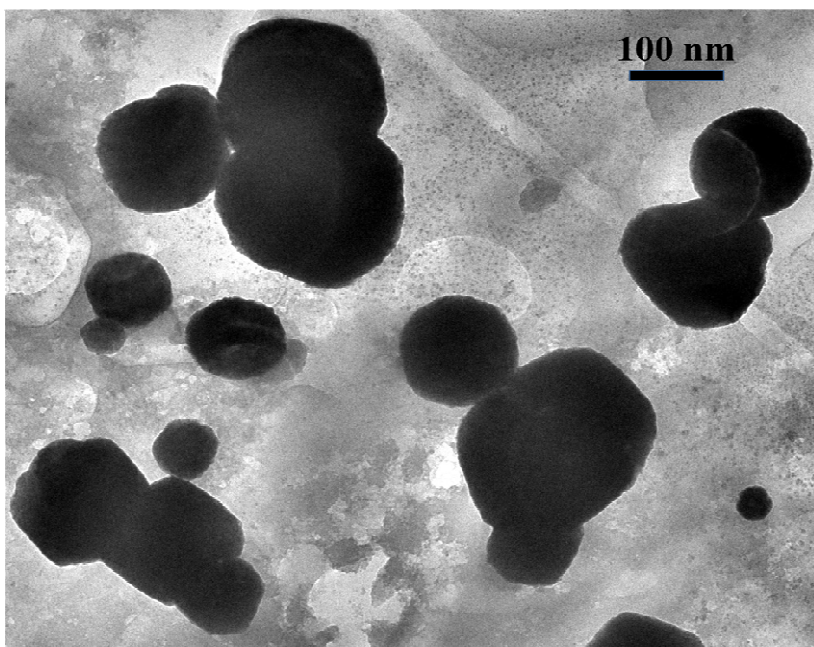


(b)

Fig. 5 Dynamic light scattering of (a) Co₃O₄-I (b) Co₃O₄-II



(a)



(b)

Fig. 6 Transmission electron microscopy images of (a) Co₃O₄-I (b) Co₃O₄-II.

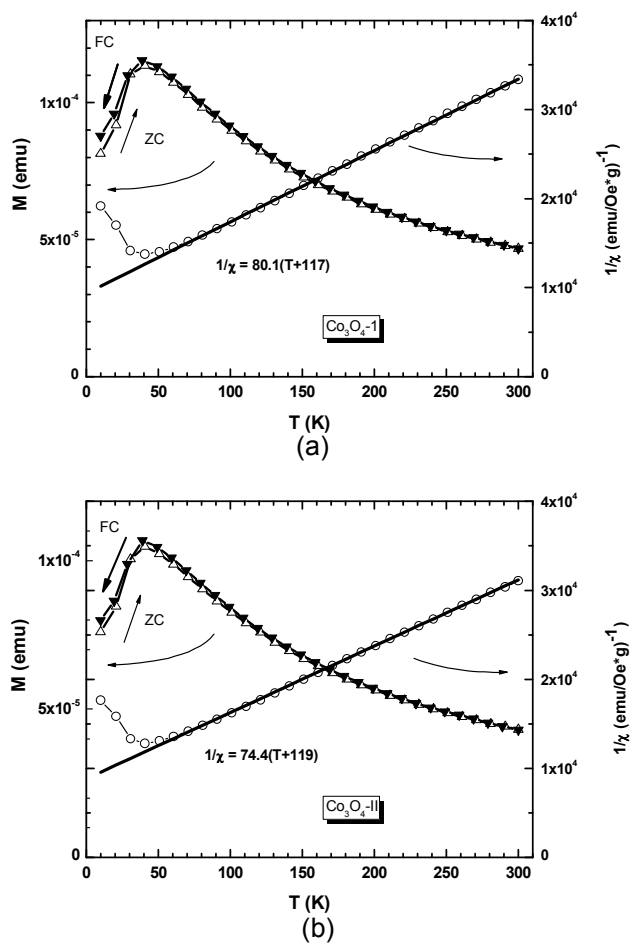
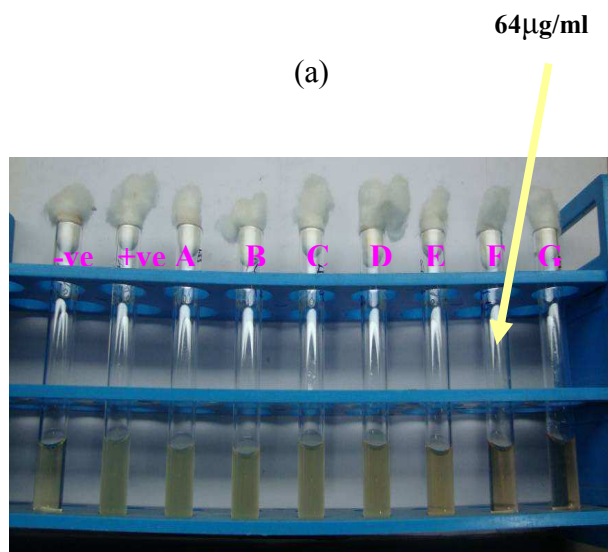


Fig. 7 The Curie-Weiss ($1/\chi - T$) plots fit well the linear line above 50 K.



(a)



(b)

Fig. 8 Minimum inhibitory concentration of $\text{Co}_3\text{O}_4\text{-I}$ nanoparticles against (a) *Staphylococcus aureus* and (b) *Escherichia coli* [Here A = 2 μ g/ml, B = 4 μ g/ml, C=8 μ g/ml, D=16 μ g/ml, E=32 μ g/ml, F=64 μ g/ml and G=128 μ g/ml.]



(a)

(b)

Fig.9 Minimum bactericidal concentration of $\text{Co}_3\text{O}_4\text{-I}$ nanoparticles against (a) *Staphylococcus aureus* and (b) *Escherichia coli* [Here A= $2\mu\text{g/ml}$, B= $4\mu\text{g/ml}$, C= $8\mu\text{g/ml}$, D= $16\mu\text{g/ml}$, E= $32\mu\text{g/ml}$, F= $64\mu\text{g/ml}$ and G= $128\mu\text{g/ml}$.]

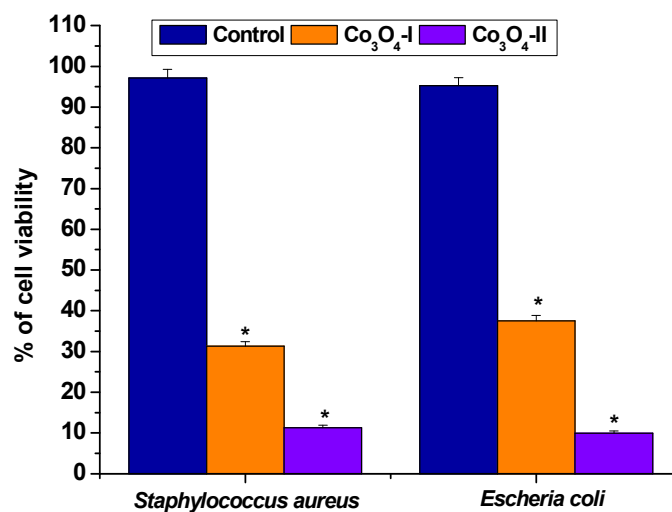


Fig. 10 Cell viability of *Staphylococcus aureus* and *Escherichia coli* due to treatment of Co_3O_4 nanoparticles. Values are expressed as the mean \pm SEM of three experiments; asterisks indicate significant differences ($P < 0.05$) compared with the control group.

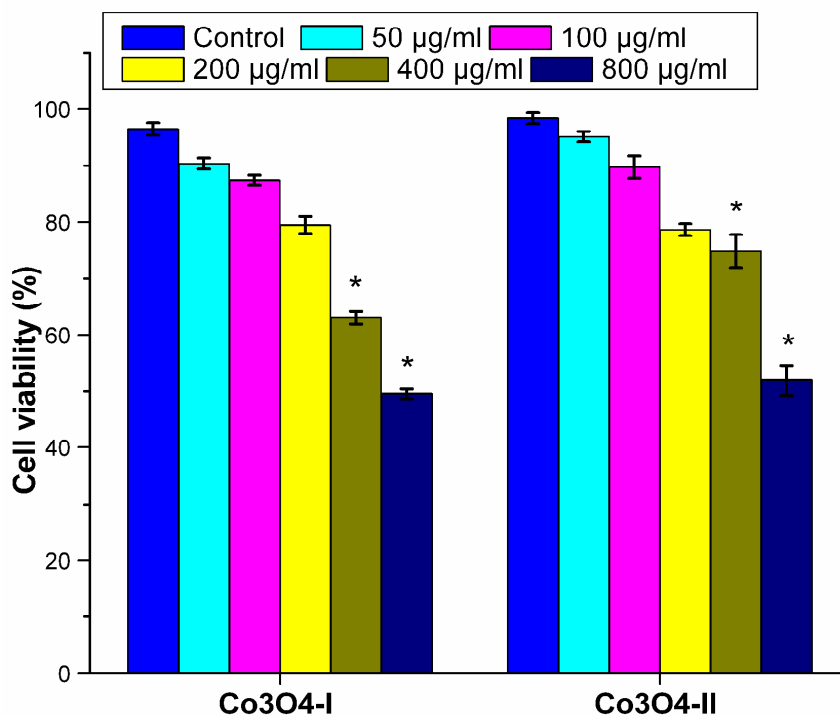


Fig. 11 Cytotoxicity of Co₃O₄ nanoparticles (50 µg/ml to 800µg/ml) against human normal Lymphocytes by MTT assay. Values are expressed as the mean ± SEM of three experiments; asterisks indicate significant differences (P<0.05) compared with the control group.

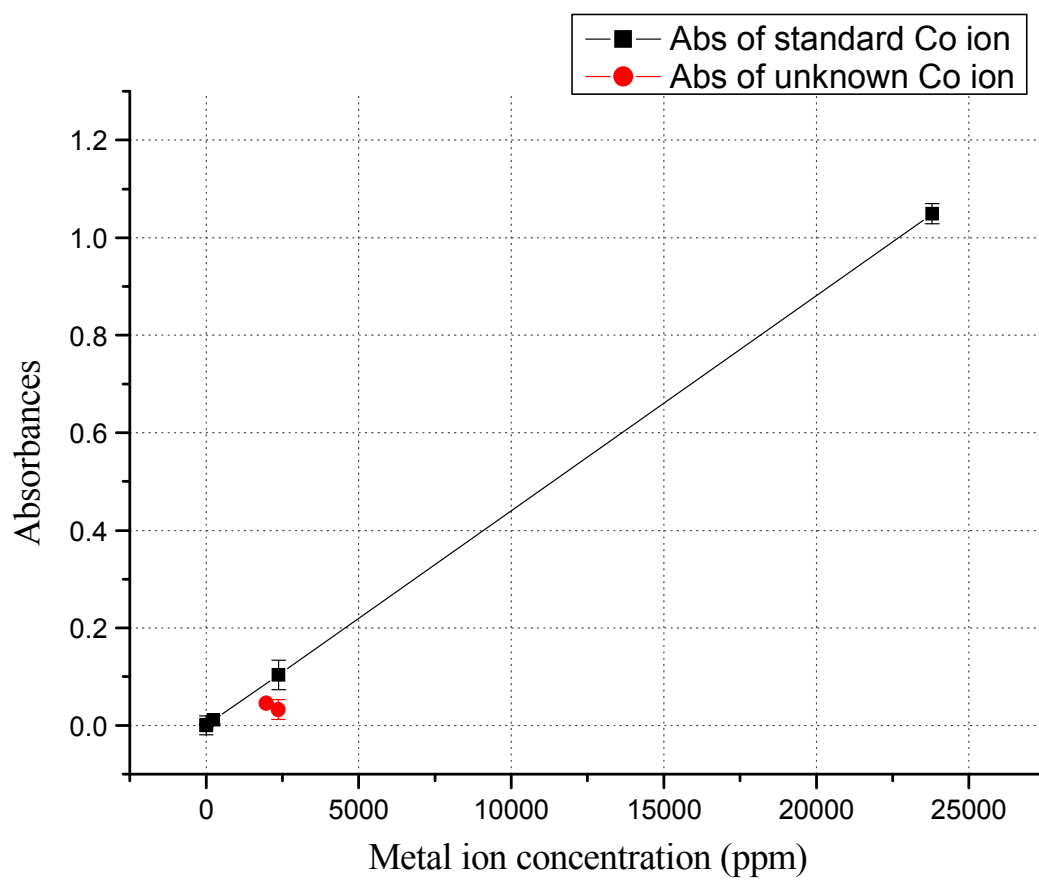


Fig. 12 Cobalt ion release assay by atomic absorption spectroscopy (AAS).

Graphical Abstract

